A high-resolution study of particle export in the southern South China Sea based on ^{234}Th:^{238}U disequilibrium

Pinghe Cai,[1] Weifang Chen,[1] Minhan Dai,[1] Zhenwen Wan,[1] Dongxiao Wang,[2] Qing Li,[1] Tiantian Tang,[1] and Dongwei Lv[1]

Received 7 April 2007; revised 29 September 2007; accepted 17 December 2007; published 17 April 2008.

[1] During a spring intermonsoon cruise in 2004, depth profiles of total and particulate ^{234}Th in the upper 100 m were collected at 36 stations in the southern South China Sea (SCS), covering a surface area of $\sim 1.0 \times 10^6$ km^2. Thorium-234 was sampled by using a modified small-volume MnO_2 co-precipitation technique, which allows mapping the ^{234}Th distribution with a high spatial resolution. A stratified structure of ^{234}Th/^{238}U disequilibria was generally observed in the upper 100 m water column, suggesting that the euphotic zone of the southern SCS in this season can be separated into two layers: an upper layer with low export production rates and a lower layer with high export production rates. At the same time, we observed extensive zones of ^{234}Th excess within the euphotic layer, which is possibly due to intense remineralization of particulate matter. Particulate organic carbon (POC) export was estimated from a three-dimensional steady state model of ^{234}Th fluxes combined with measurements of the POC/^{234}Th ratio on suspended particles. The POC export for this region varied from a low of -10.7 ± 1.5 mmolC m^{-2} d^{-1} to a high of 12.6 ± 1.1 mmolC m^{-2} d^{-1}, with an average of 3.8 ± 4.0 mmolC m^{-2} d^{-1}. A negative flux of POC export is interpreted as the result of lateral input of particulate matter from nearby waters. Regional patterns in POC export show enhanced fluxes along the western and southern boundaries of the study region, and a "tongue" of low export extending northwestward from $\sim$7°N 116°E to $\sim$10°N 111°E. This geographic distribution is consistent with the overall surface circulation pattern of the southern SCS in this season.

Citation: Cai, P., W. Chen, M. Dai, Z. Wan, D. Wang, Q. Li, T. Tang, and D. Lv (2008), A high-resolution study of particle export in the southern South China Sea based on ^{234}Th:^{238}U disequilibrium, *J. Geophys. Res.*, *113*, C04019, doi:10.1029/2007JC004268.

1. Introduction

[2] There is increasing evidence that continental margins may play a disproportionally important role in global ocean carbon cycling (for review see *Frankignoulle and Borges* [2001]; *Liu et al.* [2000]; *Tsunogai et al.* [1999]). With a relatively small surface area ($\sim$8%), continental margins contribute approximate 28% of global ocean primary production [*Eppley and Peterson*, 1979]. The net sequestration of CO_2 implies that POC export from the upper water column may be higher in the marginal sea than in the open ocean. However, constraining the magnitude of POC export in the marginal sea is difficult, due primarily to the dynamic nature of the system.

[3] The disequilibrium between ^{234}Th and ^{238}U has been widely utilized to quantify the particle scavenging and organic carbon export rates from the upper ocean [*Bacon et al.*, 1996; *Buesseler et al.*, 1992, 1998, 2006; *Buesseler*, 1998; *Coale and Bruland*, 1985, 1987; *Cochran and Masque*, 2003; *Murray et al.*, 1996; *Savoye et al.*, 2006; *Waples et al.*, 2006]. Thorium-234 is produced from the radioactive decay of ^{238}U ($t_{1/2} = 4.47 \times 10^9$ a). Since the half-life of ^{234}Th is 24.1 d, and since it is very particle reactive, the disequilibrium between its soluble parent ^{238}U and the measured ^{234}Th activity reflects the net rate of particle export from the upper ocean on timescales of days to weeks [e.g., *Buesseler et al.*, 1998; *Charette et al.*, 1999; *Rutgers van der Loeff et al.*, 2002]. In the upper ocean, both the formation of fresh particle surfaces and the packaging of particles into sinking aggregates are reflected in the observed ^{234}Th distribution.

[4] However, due to the temporal and spatial variations in the biogeochemical processes of the marginal sea, the application of ^{234}Th as a proxy of POC export therein requires at least a 2-D model to properly constrain the ^{234}Th fluxes [e.g., *Charette et al.*, 2001; *Savoye et al.*, 2006]. A single depth profile may not be representative in such an environment. In this regard, the recent development of a small-volume technique for measuring ^{234}Th in seawater has provided a more in-depth avenue of research. With the aid of a yield monitor, the technique allows one to

[1] State Key Laboratory of Marine Environmental Science, Xiamen University, Xiamen, China.
[2] Key Laboratory of Tropical Marine Environmental Dynamics, South China Sea Institute of Oceanology, Chinese Academy of Sciences, Guangzhou, China.

0148-0227/08/2007JC004268

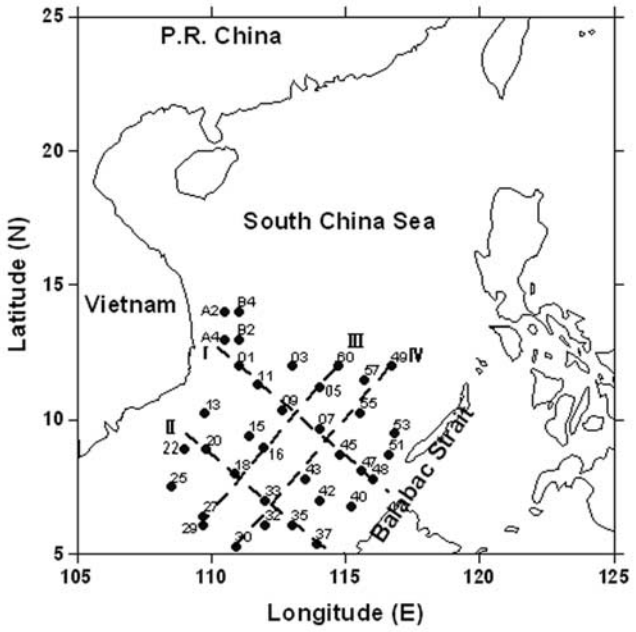

Figure 1. Map of the South China Sea. Sampling stations from the spring intermonsoon cruise in 2004 are indicated by solid cycles. Four sections are indicated by the dash lines (line I: transect A4-48; line II: transect 22–37; line III: transect 29-60; line IV: transect 30–49).

achieve high-resolution, high-precision depth profiles of ^{234}Th [*Benitez-Nelson et al.*, 2001a, 2001b; *Buesseler et al.*, 2001; *Cai et al.*, 2006a; *Pike et al.*, 2005]. The application of this technique at the Hawaii Ocean Time series (HOT) Station ALOHA and in the Southern Ocean Iron Experiment (SOFeX) has revealed a refined temporal and spatial structure of ^{234}Th that had not been previously identified by using typical snapshot sampling techniques [*Benitez-Nelson et al.*, 2001a; *Buesseler et al.*, 2005]. Such high-resolution applications, however, have yet to be reported in marginal seas.

[5] In this study, we attempt to examine the dynamics of the ^{234}Th distribution and to quantify POC export during the intermonsoon season in the southern South China Sea by using this small-volume technique. Thirty-six profiles of ^{234}Th spanning an area of $\sim$1.0 $\times$ 10^6 km^2 were obtained, such that we are able to, for the first time, construct high-resolution, high-precision spatial distributions of ^{234}Th and hence POC export in this region.

2. Sampling and Analyses

2.1. Study Area

[6] The South China Sea (SCS) is one of the largest marginal seas in the world with an area of 3.5 $\times$ 10^6 km^2 and an average depth of about 1350 m. The sea is notable for its shallow mixed layer, which is less than 50 m most of the year. It is also a region of strong seasonal reversals in surface circulation driven by monsoonal winds. These physical processes are postulated to support seasonally high primary production levels due to the enhancement of nutrient supply. Observations and models in this region generally support this hypothesis [*Liu et al.*, 2002; *Ning et al.*, 2004]. Seasonal patterns in surface production are thought to drive the strong seasonal variations in deep particle fluxes observed in the South China Sea sediment trap moorings [*Chen et al.*, 1998]. Little is known, however, regarding the spatial variations in shallow particle fluxes and how these respond to physical and biological processes in this region.

2.2. Sample Collection

[7] The samples were collected during a spring intermonsoon cruise to the southern SCS from 28 April to 25 May in 2004 on board R/V "Shiyan 3" from the Chinese Academy of Sciences. A total of 36 stations were occupied during this cruise. The cruise tracks (Figure 1) started with station A2 offshore of Vietnam, headed to the southernmost station, 30, and followed the eastern boundary of the sea back to station B4. Stations were sampled in the order as arranged in Table 1. For most stations, samples were collected throughout the upper 100 m at 0, 25, 50, 75, 100 m. For a few stations (Station 22, 25, 27, 29, and 30) where bottom depth falls in the range of 100–150 m, samples at 100 m were not collected in order to minimize the influence of sediment re-suspension on the estimates of upper ocean POC export. Samples for ^{234}Th and POC were collected at the same depth using Niskin bottles attached on a CTD rosette sampler. A volume of 2 L of seawater was used to determine the total ^{234}Th activities. For the measurements of particulate ^{234}Th and POC, 6–8 L of seawater was filtered onto a 25 mm diameter, 1 μm pore size quartz fiber filter (QMA, Whatman).

2.3. Thorium-234 Analyses

[8] Analysis for total ^{234}Th in 2-L samples was based on the small-volume MnO_2 co-precipitation technique following the procedure described by *Buesseler et al.* [2001] and *Cai et al.* [2006a]. Briefly, within 1 h of collection, unfiltered 2-L samples were acidified to pH $\approx$ 2 with 3 mL of concentrated HNO_3. Approximately 10 dpm of ^{230}Th was added as a yield tracer. The samples were mixed thoroughly and allowed to equilibrate for >12 h. Upon equilibration, pH was brought back to 8.0–8.15 with concentrated NH_4OH. Then, 0.25 mL of $KMnO_4$ solution (3.0 g l^{-1}) and 0.25 mL of $MnCl_2$ solution (8.0 g $MnCl_2 \cdot 4H_2O$ l^{-1}) were added to form a suspension of MnO_2. After the samples were heated in a water bath (>80°C) for 2 h and allowed to cool, the suspension was filtered onto a 25 mm diameter, 1 μm pore size QMA filter. It has been demonstrated that the heating step dramatically reduces the filtration time for MnO_2 precipitates and hence makes this novel small-volume technique more applicable in the field [*Cai et al.*, 2006a]. Finally, the filtered MnO_2 precipitates were dried and mounted under one layer of Mylar film and two layers of aluminum foil for beta counting.

[9] Particulate samples collected on QMA filters were dried overnight at 60 °C and prepared for beta counting with Mylar and aluminum covers identical to those used for total ^{234}Th samples. All samples were beta-counted 5 times with a gas-flow proportional low-level RISØ beta counter (Model GM-5-25, RISØ National Laboratory) over a period of >150 days in order to follow the decay of ^{234}Th. For the first run of measurements, samples were counted for 700 min or until the counting error was <3%. A two-component fitting technique was applied to find the best fit of gross-counting

Table 1. Temperature, Salinity, ^{234}Th and ^{238}U Activities, and POC Concentration in the Upper Southern South China Sea

Depth, m	T, °C	S (PSU)	$^{234}Th_p$, dpm l^{-1}	$^{234}Th_T$, dpm l^{-1}	^{238}U, dpm l^{-1}	POC, μmol l^{-1}
A2, 14°00′N, 110°30′E, 1795 m						
0	29.42	33.73	0.09 ± 0.01	2.37 ± 0.08	2.39	2.1
25	27.34	33.60	0.46 ± 0.01	2.32 ± 0.13	2.38	2.8
50	22.09	34.35	0.11 ± 0.01	1.45 ± 0.08	2.43	3.1
75	21.06	34.51	0.28 ± 0.02	1.61 ± 0.07	2.44	2.9
100	20.13	34.59	0.23 ± 0.01	1.59 ± 0.08	2.45	1.4
A4, 13°00′N, 110°30′E, 2600 m						
0	29.70	33.82	0.13 ± 0.01	2.67 ± 0.13	2.39	1.9
25	29.52	33.82	0.28 ± 0.04	2.08 ± 0.11	2.39	3.5
50	26.92	33.73	0.37 ± 0.02	1.90 ± 0.07	2.39	2.6
75	20.30	34.54	0.40 ± 0.02	1.93 ± 0.09	2.45	2.4
100	17.55	34.60	0.29 ± 0.01	2.20 ± 0.07	2.45	1.7
01, 12°00′N, 111°00′E, 2886 m						
0	29.55	33.85	0.14 ± 0.02	2.27 ± 0.13	2.40	2.9
25	27.62	33.91	0.26 ± 0.01	1.84 ± 0.10	2.40	2.4
50	23.82	34.17	0.42 ± 0.02	1.78 ± 0.08	2.42	2.0
75	21.25	34.52	0.22 ± 0.01	1.84 ± 0.10	2.44	2.1
100	17.97	34.64	0.23 ± 0.01	2.59 ± 0.10	2.45	1.5
09, 10°22′N, 112°39′E, 1550 m						
0	29.70	33.77	0.13 ± 0.01	2.34 ± 0.14	2.39	2.7
25	29.67	33.76	0.20 ± 0.02	2.20 ± 0.09	2.39	2.0
50	25.60	33.79	0.31 ± 0.02	2.08 ± 0.11	2.39	1.6
75	22.66	34.34	0.34 ± 0.01	1.66 ± 0.09	2.43	2.9
100	20.58	34.53	0.23 ± 0.02	2.41 ± 0.13	2.45	1.3
07, 09°41′N, 114°00′E, 1556 m						
0	29.95	33.88	0.16 ± 0.02	2.11 ± 0.11	2.40	2.2
25	29.79	33.88	0.21 ± 0.02	1.95 ± 0.10	2.40	2.0
50	28.42	33.68	0.28 ± 0.03	2.25 ± 0.10	2.38	2.2
75	23.16	34.27	0.39 ± 0.02	2.06 ± 0.08	2.43	2.3
100	19.74	34.53	0.22 ± 0.02	2.32 ± 0.12	2.45	1.1
11, 11°18′N, 111°42′E, 1552 m						
0	29.87	33.79	0.09 ± 0.01	1.92 ± 0.11	2.39	1.6
25	28.36	33.75	0.22 ± 0.01	2.23 ± 0.10	2.39	1.6
50	23.17	34.39	0.54 ± 0.03	1.98 ± 0.07	2.43	2.6
75	21.35	34.52	0.22 ± 0.01	1.96 ± 0.07	2.44	3.0
100	20.48	34.56	0.19 ± 0.01	2.32 ± 0.09	2.45	1.3
13, 10°15′N, 109°45′E, 1060 m						
0	29.76	33.77	0.14 ± 0.01	2.35 ± 0.12	2.39	2.0
25	25.57	33.88	0.28 ± 0.01	2.36 ± 0.08	2.40	2.8
50	24.43	34.17	0.30 ± 0.02	2.15 ± 0.09	2.42	1.0
75	22.72	34.45	0.19 ± 0.01	2.06 ± 0.07	2.44	2.9
100	21.11	34.48	0.22 ± 0.01	2.29 ± 0.14	2.44	1.5
15, 09°24′N, 111°23′E, 1750 m						
0	29.82	33.82	0.13 ± 0.02	2.12 ± 0.08	2.39	2.0
25	29.83	33.81	—	2.25 ± 0.11	2.39	—
50	27.10	33.94	—	1.90 ± 0.09	2.40	—
75	23.53	34.24	—	1.83 ± 0.10	2.42	—
100	21.60	34.41	0.24 ± 0.02	2.46 ± 0.12	2.44	0.4
16, 08°57′N, 111°56′E, 1510 m						
0	29.82	33.85	0.13 ± 0.01	2.28 ± 0.09	2.40	2.5
25	29.72	33.82	0.23 ± 0.02	2.99 ± 0.11	2.39	1.5
50	25.29	34.07	0.38 ± 0.03	2.67 ± 0.15	2.41	2.0
75	23.22	34.31	0.37 ± 0.02	2.81 ± 0.15	2.43	2.5
100	22.26	34.38	0.24 ± 0.02	2.52 ± 0.08	2.43	0.8
18, 08°00′N, 110°51′E, 1908 m						
0	30.14	33.62	0.15 ± 0.01	2.19 ± 0.12	2.38	3.1
25	29.86	33.64	0.17 ± 0.02	2.01 ± 0.11	2.38	2.5
50	24.70	33.97	0.21 ± 0.02	2.11 ± 0.09	2.41	1.3
75	22.58	34.29	0.18 ± 0.01	1.87 ± 0.07	2.43	2.6
100	21.01	34.48	0.24 ± 0.02	2.25 ± 0.08	2.44	1.9
20, 08°54′N, 109°47′E, 1688 m						
0	29.86	33.74	0.15 ± 0.01	2.35 ± 0.10	2.39	1.7
25	29.74	33.71	0.16 ± 0.02	2.06 ± 0.08	2.39	2.3
50	23.52	34.20	0.17 ± 0.02	1.79 ± 0.12	2.42	2.1
75	21.85	34.38	0.16 ± 0.03	2.22 ± 0.09	2.43	2.0
100	20.45	34.52	0.27 ± 0.02	2.31 ± 0.09	2.44	1.9
22, 08°54′N, 109°00′E, 140 m						
0	29.85	33.75	0.14 ± 0.01	2.33 ± 0.13	2.39	2.3
25	29.52	33.73	0.15 ± 0.01	2.25 ± 0.13	2.39	3.1
50	24.09	34.14	0.18 ± 0.02	1.73 ± 0.08	2.42	2.3
75	22.36	34.37	0.23 ± 0.02	1.82 ± 0.07	2.43	2.2

Table 1. (continued)

Depth, m	T, °C	S (PSU)	$^{234}Th_p$, dpm l^{-1}	$^{234}Th_T$, dpm l^{-1}	^{238}U, dpm l^{-1}	POC, μmol l^{-1}
25, 07°30′N, 108°29′E, 106 m						
0	30.10	33.52	0.11 ± 0.02	2.31 ± 0.12	2.37	2.8
25	29.34	33.62	0.15 ± 0.01	2.05 ± 0.11	2.38	2.7
50	24.31	34.09	0.32 ± 0.01	2.32 ± 0.11	2.41	2.6
75	21.35	34.45	0.29 ± 0.02	1.86 ± 0.07	2.44	2.3
27, 06°24′N, 109°42′E, 110 m						
0	30.02	33.37	0.13 ± 0.01	2.28 ± 0.11	2.38	2.7
25	29.84	33.53	0.16 ± 0.01	2.25 ± 0.12	2.39	2.6
50	23.02	34.31	0.27 ± 0.02	1.94 ± 0.11	2.41	2.1
75	21.16	34.47	0.22 ± 0.01	2.18 ± 0.09	2.43	1.7
29, 06°05′N, 109°40′E, 153 m						
0	29.61	33.37	0.08 ± 0.02	2.14 ± 0.10	2.36	3.2
25	26.56	34.02	0.17 ± 0.01	2.20 ± 0.08	2.41	2.0
50	22.46	34.25	0.36 ± 0.03	2.04 ± 0.11	2.36	2.5
75	21.68	34.44	0.18 ± 0.01	1.82 ± 0.09	2.44	1.4
30, 05°18′N, 110°54′E, 140 m						
0	29.90	33.70	0.11 ± 0.01	2.39 ± 0.12	2.39	2.5
25	28.30	33.79	0.15 ± 0.01	2.04 ± 0.08	2.39	2.3
50	23.26	34.27	0.25 ± 0.02	1.71 ± 0.10	2.43	2.9
75	20.73	34.50	0.21 ± 0.02	2.18 ± 0.10	2.44	1.9
32, 06°06′N, 112°01′E, 1550 m						
0	29.55	34.02	0.20 ± 0.02	2.09 ± 0.12	2.41	6.0
25	28.14	33.84	0.18 ± 0.02	2.24 ± 0.07	2.40	2.3
50	23.33	34.27	0.31 ± 0.03	2.10 ± 0.09	2.43	2.6
75	21.49	34.42	0.16 ± 0.01	2.26 ± 0.10	2.44	1.9
100	19.12	34.56	0.21 ± 0.01	2.42 ± 0.11	2.45	1.9
33, 07°00′N, 112°00′E, 2040 m						
0	29.44	33.99	0.15 ± 0.02	2.70 ± 0.12	2.41	3.1
25	29.46	34.02	0.17 ± 0.01	2.01 ± 0.08	2.41	2.9
50	26.18	34.08	0.43 ± 0.02	2.12 ± 0.08	2.41	2.7
75	23.19	34.30	0.29 ± 0.02	2.34 ± 0.10	2.43	2.3
100	20.35	34.55	0.21 ± 0.01	3.23 ± 0.12	2.45	1.2
35, 06°06′N, 113°00′E, 1476 m						
0	29.14	33.85	0.17 ± 0.01	2.01 ± 0.07	2.40	2.8
25	28.85	33.90	0.18 ± 0.01	2.20 ± 0.08	2.40	2.0
50	23.18	34.28	0.27 ± 0.01	2.48 ± 0.10	2.43	2.5
75	21.57	34.40	0.18 ± 0.03	2.38 ± 0.08	2.44	1.7
100	19.67	34.52	0.28 ± 0.01	2.33 ± 0.10	2.44	2.2
37, 05°24′N, 113°54′E, 1298 m						
0	29.33	33.56	0.11 ± 0.01	2.14 ± 0.10	2.38	3.2
25	28.59	33.58	0.17 ± 0.02	2.01 ± 0.12	2.38	2.9
50	24.49	34.12	0.36 ± 0.02	1.98 ± 0.07	2.42	3.2
75	22.51	34.36	0.31 ± 0.01	2.32 ± 0.06	2.43	2.0
100	20.66	34.49	0.18 ± 0.01	2.34 ± 0.10	2.44	1.5
40, 06°48′N, 115°12′E, 1386 m						
0	28.77	33.52	0.15 ± 0.01	1.54 ± 0.09	2.37	4.5
25	29.01	33.82	0.15 ± 0.01	2.39 ± 0.07	2.39	3.4
50	25.37	33.95	0.23 ± 0.01	2.77 ± 0.12	2.40	2.3
75	21.64	34.41	0.37 ± 0.03	3.44 ± 0.16	2.44	3.6
100	20.53	34.47	0.25 ± 0.01	3.13 ± 0.19	2.44	2.6
42, 07°00′N, 114°01′E, 2083 m						
0	28.98	33.83	0.21 ± 0.02	1.64 ± 0.10	2.40	8.7
25	27.85	34.13	0.22 ± 0.01	1.67 ± 0.08	2.42	2.5
50	23.02	34.30	0.43 ± 0.02	1.99 ± 0.09	2.43	1.7
75	22.31	34.35	0.23 ± 0.02	2.62 ± 0.10	2.43	2.4
100	20.62	34.44	0.23 ± 0.02	2.44 ± 0.11	2.44	1.1
43, 07°48′N, 113°30′E, 1728 m						
0	29.25	33.64	0.15 ± 0.02	2.18 ± 0.13	2.38	2.9
25	29.25	33.67	0.17 ± 0.01	2.11 ± 0.10	2.38	1.5
50	25.05	34.02	0.43 ± 0.03	2.29 ± 0.14	2.41	0.8
75	21.98	34.40	0.29 ± 0.02	2.44 ± 0.15	2.44	1.7
100	19.00	34.52	0.21 ± 0.02	2.48 ± 0.10	2.44	0.8
45, 08°43′N, 114°49′E, 2307 m						
0	29.38	33.65	0.16 ± 0.01	2.22 ± 0.13	2.38	1.7
25	27.88	33.66	0.20 ± 0.02	2.06 ± 0.09	2.38	2.7
50	23.58	34.22	0.51 ± 0.05	2.19 ± 0.10	2.42	3.0
75	20.82	34.48	0.26 ± 0.02	2.45 ± 0.14	2.44	1.7
100	19.01	34.54	0.22 ± 0.02	2.52 ± 0.15	2.45	0.8
47, 08°07′N, 115°35′E, 2897 m						
0	29.29	34.07	0.14 ± 0.01	2.22 ± 0.13	2.41	1.4
25	29.26	34.07	0.16 ± 0.01	2.00 ± 0.09	2.41	2.1
50	24.39	34.14	0.28 ± 0.02	2.29 ± 0.11	2.42	2.0
75	22.25	34.36	0.29 ± 0.02	2.42 ± 0.12	2.43	1.6

Table 1. (continued)

Depth, m	T, °C	S (PSU)	$^{234}Th_p$, dpm l^{-1}	$^{234}Th_T$, dpm l^{-1}	^{238}U, dpm l^{-1}	POC, μmol l^{-1}
100	20.71	34.48	0.25 ± 0.01	2.64 ± 0.14	2.44	1.4
48, 07°49′N, 116°00′E, 2438 m						
0	28.47	33.54	0.13 ± 0.01	2.19 ± 0.13	2.38	2.3
25	27.39	33.97	0.15 ± 0.01	1.94 ± 0.09	2.41	2.7
50	24.30	34.14	0.24 ± 0.01	1.87 ± 0.11	2.42	1.7
75	22.92	34.30	0.25 ± 0.02	2.30 ± 0.12	2.43	1.2
100	20.35	34.49	0.22 ± 0.02	2.54 ± 0.13	2.44	0.8
51, 08°43′N, 116°36′E, 2297 m						
0	29.55	33.78	0.15 ± 0.01	1.98 ± 0.09	2.39	2.0
25	29.37	33.79	0.17 ± 0.02	2.29 ± 0.11	2.39	2.6
50	23.96	34.16	0.39 ± 0.03	2.20 ± 0.09	2.42	1.6
75	21.65	34.42	0.30 ± 0.02	2.56 ± 0.09	2.44	2.0
100	19.82	34.51	0.25 ± 0.01	2.54 ± 0.12	2.44	1.1
53, 09°31′N, 116°49′E, 2092 m						
0	29.75	33.85	0.16 ± 0.01	2.38 ± 0.09	2.40	0.9
25	29.61	33.84	0.20 ± 0.02	2.26 ± 0.12	2.40	1.5
50	26.71	33.89	0.51 ± 0.05	2.20 ± 0.11	2.40	2.1
75	21.57	34.43	0.26 ± 0.02	2.21 ± 0.09	2.44	2.2
100	20.16	34.49	0.22 ± 0.02	2.33 ± 0.13	2.44	1.2
55, 10°17′N, 115°33′E, 1839 m						
0	30.04	33.97	0.15 ± 0.01	2.26 ± 0.12	2.41	2.2
25	29.82	33.96	0.15 ± 0.02	1.80 ± 0.07	2.40	2.1
50	25.55	33.99	0.33 ± 0.02	2.00 ± 0.10	2.41	2.3
75	22.53	34.34	0.36 ± 0.02	2.15 ± 0.13	2.43	0.5
100	19.70	34.51	0.24 ± 0.02	2.48 ± 0.10	2.44	1.2
57, 11°30′N, 115°42′E, 3698 m						
0	30.10	33.87	0.17 ± 0.02	2.16 ± 0.11	2.40	2.0
25	30.09	33.87	0.17 ± 0.01	1.88 ± 0.10	2.40	4.4
50	27.31	33.76	0.40 ± 0.02	1.97 ± 0.10	2.39	2.2
75	22.23	34.35	0.41 ± 0.01	1.78 ± 0.11	2.43	3.7
100	20.36	34.50	0.30 ± 0.01	2.63 ± 0.09	2.44	3.4
49, 12°01′N, 116°42′E, 2707 m						
0	30.10	33.78	0.13 ± 0.01	2.38 ± 0.13	2.39	1.9
25	27.85	33.55	0.24 ± 0.02	1.93 ± 0.12	2.38	1.4
50	27.03	33.65	0.35 ± 0.02	2.28 ± 0.13	2.38	2.4
75	21.84	34.34	0.38 ± 0.03	2.18 ± 0.11	2.43	1.9
100	19.32	34.53	0.20 ± 0.02	2.43 ± 0.14	2.44	1.7
60, 12°00′N, 114°42′E, 4368 m						
0	30.11	33.71	0.11 ± 0.01	2.35 ± 0.09	2.39	1.9
25	30.12	33.71	0.13 ± 0.02	2.13 ± 0.11	2.38	2.2
50	27.17	33.58	0.32 ± 0.01	2.46 ± 0.08	2.38	1.4
75	22.02	34.40	0.42 ± 0.03	2.43 ± 0.11	2.42	2.2
100	19.27	34.55	0.18 ± 0.02	2.62 ± 0.09	2.44	1.2
05, 11°12′N, 114°00′E, 3746 m						
0	29.84	33.64	0.18 ± 0.01	2.35 ± 0.14	2.38	3.4
25	29.72	33.69	0.20 ± 0.01	2.09 ± 0.11	2.38	0.6
50	26.48	33.70	0.54 ± 0.02	2.22 ± 0.07	2.39	2.3
75	21.99	34.42	0.35 ± 0.02	2.34 ± 0.12	2.44	2.3
100	19.14	34.55	0.23 ± 0.01	2.74 ± 0.10	2.44	1.8
03, 12° 01′ N, 113° 01′E, 4300 m						
0	29.24	33.73	0.16 ± 0.01	2.33 ± 0.11	2.39	2.4
25	29.25	33.73	—	2.18 ± 0.10	2.39	—
50	27.30	33.69	—	2.32 ± 0.08	2.39	—
100	20.01	34.49	0.32 ± 0.01	2.51 ± 0.12	2.44	1.2
B2, 13°01′N, 111°00′E, 3698 m						
0	29.54	33.74	0.16 ± 0.01	2.68 ± 0.11	2.39	2.1
25	29.51	33.74	0.15 ± 0.01	2.23 ± 0.10	2.39	1.6
50	26.47	33.73	0.36 ± 0.02	2.16 ± 0.10	2.39	1.9
75	21.85	34.39	0.42 ± 0.01	2.45 ± 0.11	2.44	2.4
100	19.33	34.53	0.30 ± 0.02	2.43 ± 0.14	2.45	1.5
B4, 14°00′N, 111°00′E, 2280 m						
0	29.70	33.76	0.14 ± 0.01	2.37 ± 0.10	2.39	2.9
25	28.66	33.65	0.15 ± 0.01	2.32 ± 0.09	2.39	2.4
50	23.86	34.16	0.36 ± 0.02	2.18 ± 0.07	2.40	3.7
75	20.99	34.52	0.66 ± 0.04	2.21 ± 0.13	2.44	2.8
100	18.66	34.60	0.32 ± 0.01	2.70 ± 0.10	2.45	1.9

data to an exponential curve with a half-life of 24.1 days. Each time point was further weighed by the individual counting uncertainty (SigmaPLOT™). The net count rate of ^{234}Th at the midpoint of sample filtration, as well as the background count rate, was estimated. The background count rates determined from the curve regression for the total ^{234}Th and the particulate samples are 0.43 ± 0.05 cpm and 0.29 ± 0.06 cpm respectively, which include the detector back-

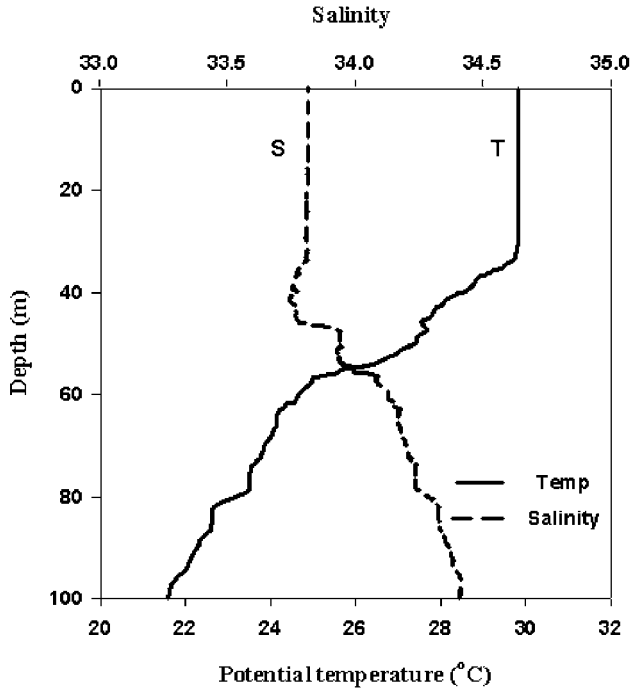

Figure 2. Vertical distributions of potential temperature (T) and salinity (S) from the upper 100 m at Station 15 in the southern South China Sea.

ground (0.1∼0.2 cpm). After counting, the MnO_2 precipitates were disassembled and placed in 100 mL Teflon beakers for recovery assessment. Recovery assessment was possible because 10 dpm of ^{228}Th was added to the MnO_2 precipitates prior to radiochemical purification for recovery determination. The subsequent procedure for the isolation of Th isotopes was conducted according to *Cai et al.* [2006a]. Finally, Th was extracted into a 0.25 M Theonyl trifluoroacetone (TTA)/benzene solution, and evaporated onto a stainless steel disc. The discs were counted by alpha spectrometry in ultra ion-planted detectors (Octête ^{TM} PC) until the uncertainty of ^{230}Th/^{228}Th ratio was lower than 3%. Results showed that recoveries were generally greater than 85% with an average of 90.9 ± 4.3% for these samples (n = 150). Recoveries below 85% ranged from 23.8% to 84.7% with a mean of 71.9 ± 17.4% (n = 23). Low recoveries were likely caused by the organic complexation of ^{234}Th as well as physical loss of the MnO_2 precipitate during sample processing. Corrections were applied to ^{234}Th activity calculations on the basis of ^{230}Th recoveries. All data were decay corrected to the time of collection and reported with a propagated uncertainty that includes the standard uncertainty associated with the ^{234}Th fitting curve and 1 sigma counting uncertainty from the recovery measurements. Detector calibration for the total and particulate ^{234}Th samples was carried out using aged seawater as described by *Cai et al.* [2006b]. The average counting efficiency for samples covered with one layer of Mylar film and two layers of aluminum foil (with a density of 3.6 mg cm^{-2}) was 0.50 ± 0.01 and varied by <2% among detectors. Uranium-238 activities were estimated from salinity measurements using a calibrated CTD and the relationship of ^{238}U (dpm l^{-1}) = 0.0686 × salinity × density [*Chen et al.*, 1986].

2.4. POC Analyses

[10] After beta counting, the particulate samples were then used to determine POC concentration. In this study, we use the term POC to refer to the fraction retained on the 1.0 μm QMA filter, as it is closest in practice to the commonly used GF/F filters with a nominal 0.7 μm cut-off. POC concentrations were determined with a PE-2400 SERIES II CHNS/O analyzer according to the JGOFS protocols [*Knap et al.*, 1996]. All samples were treated via acid fuming to remove carbonate. Each sample was corrected for a C blank. The C blank of the filter was less than 6 μg C, which on average, accounted for ∼5% of the POC on the QMA filters. On the basis of replicate analyses, the precision for the POC determination was <10%.

3. Results

[11] Thorium-234 activity, POC concentration as well as potential temperature (T) and salinity (S) in the upper southern SCS are presented in Table 1. In an attempt to examine regional and depth-related variations in the data, all data were contoured by a software package (SURFER^{TM} by Golden Software), which utilizes a linear kriging technique to grid the data. Temporal variations are ignored within the 4-week time period required to cover the study region.

3.1. Hydrography

[12] Depth profiles of T and S indicate a well stratified water column in the upper southern SCS in this season with an average mixed layer depth of 27 ± 7 m. The mixed layer depth is deeper westward (Figure not shown). Here, the mixed layer is defined by using a density-based criterion with the difference of 0.5°C from the reference layer [*Kara et al.*, 2000]. As an example, Figure 2 shows a typical type of the depth profiles of T and S, at Station 15. Regional patterns of T and S at 0 and 50 m depth horizons are shown in Figure 3. At the surface, a low temperature, low salinity water mass extended northwestward from Balabac Strait to ∼8°N 112°E. The occurrence of the low temperature, low salinity plume in this regime has been recorded historically, and is thought to be associated with the intrusion of surface water from the Sulu Sea through the Balabac Strait [*Huang*, 1994]. In the southwest, a high temperature, low salinity plume was observed. This plume could be the result of freshwater input from Mekong River [*Hu et al.*, 2000].

[13] During the cruise, the general pattern in circulation shows a basin-wide anti-cyclonic gyre in the most water in the southern SCS, evident as warm upper water in the interior while cold water surrounding (Figure 3, temperature at 50 m level). This pattern results from the monsoon-associated anti-cyclonic wind stress curl. In addition, there are several meso-scale eddies formed in the western and southern parts of the study domain. For instance, there is a cold eddy off the southwest Vietnam. Historical observations have shown that the NE monsoon could lead to the pileup of surface water over the southwestern shelves of the SCS. During the spring, the NE monsoon collapses and the surface water recedes, resulting in enhanced upwelling

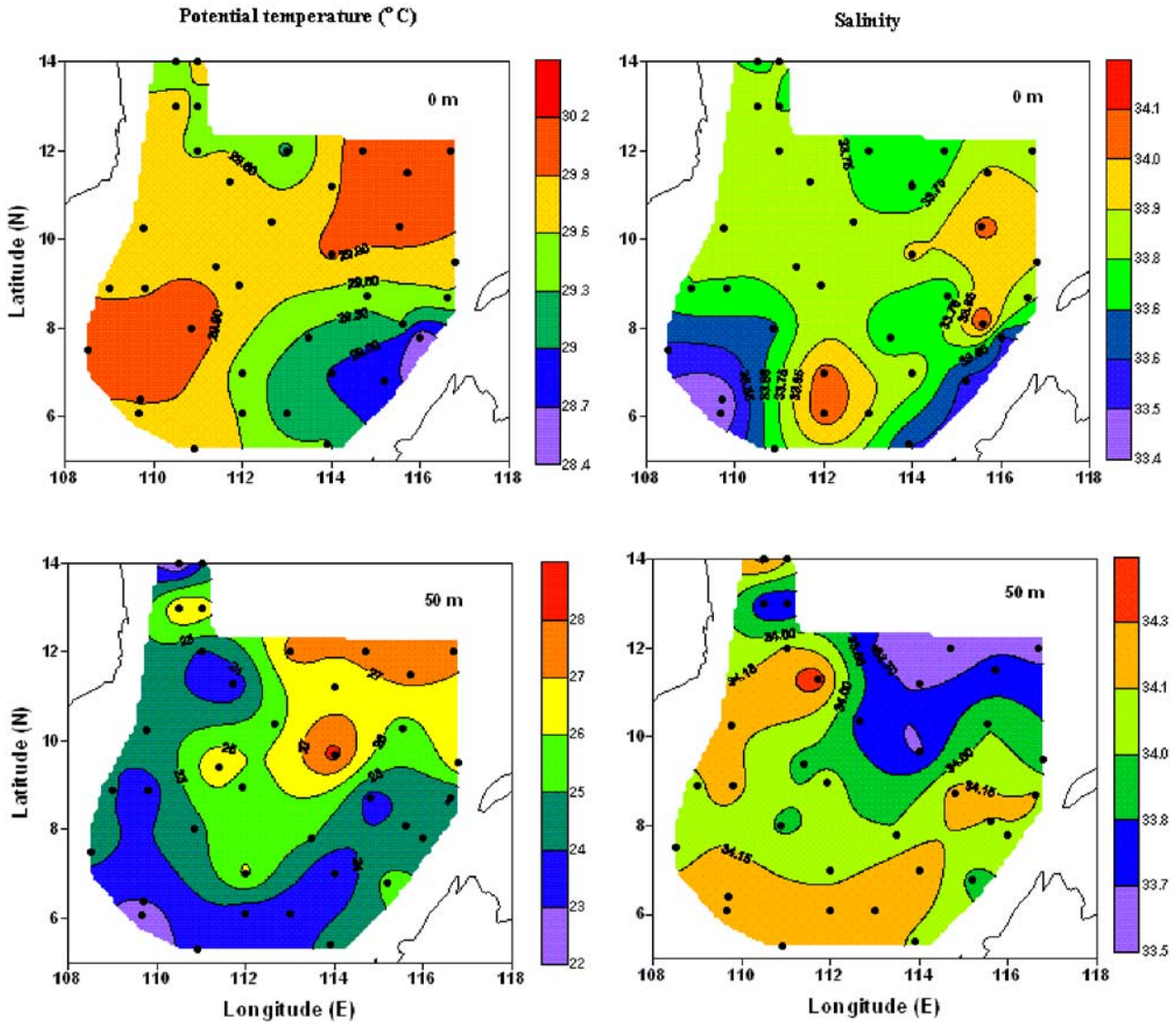

Figure 3. Contour plots of potential temperature (left panels) and salinity (right panels) at typical depth horizons (0 and 50 m) in the southern South China Sea.

of low temperature, high salinity water from depth [e.g., *Hu et al.*, 2000].

3.2. Depth-Related Variability in ^{234}Th Activities

[14] Substantial regional and depth-related variations in the total and particulate ^{234}Th activities are observed. Total ^{234}Th activities ranged from a low of 1.54 ± 0.09 dpm l^{-1} to a high of 3.44 ± 0.16 dpm l^{-1}. Particulate ^{234}Th activities varied between 0.08 ± 0.02 dpm l^{-1} and 0.66 ± 0.04 dpm l^{-1}, accounting for <5–27% of the total ^{234}Th activity (Table 1). Plotted in Figure 4 are typical transects showing depth distributions of total and particulate ^{234}Th. Four transects are indicated by the dash lines in the Figure 1. The NW-SE transects A4-48 and 22-37 consist of A4, 01, 11, 09, 07, 45, 47, 48, and 22, 20, 18, 33, 35, 37, respectively. The NE-SW transects 60-29 and 49-30, meanwhile, comprise 29, 27, 18, 16, 09, 05, 60 and 30, 32, 33, 43, 45, 55, 57, 49, respectively. As illustrated in Figure 4, surface total ^{234}Th activities were, in general, slightly lower than, or within errors equal to ^{238}U activities. Below, a remarkable decrease in ^{234}Th activities was generally evident, indicating significant particle export in the subsurface layer. At 100 m, ^{234}Th activities approached secular equilibrium with ^{238}U. The average total ^{234}Th activity at 100 m during the sampling was within 1% of equilibrium with ^{238}U, though some samples were found to have either significant depletion or excess ^{234}Th. As a consequence, a stratified structure of ^{234}Th/^{238}U disequilibria was evident in the euphotic zone, which is defined as the penetration depth of 1% light, and mostly located at ~75–100 m [*Liu et al.*, 2001]. It suggests that during the intermonsoon, the euphotic zone of the southern SCS can be separated into two layers: an upper layer characterized by low export production rates, low net scavenging, and long dissolved ^{234}Th residence times; and a subsurface with higher export production values, more intensive scavenging, and shorter dissolved ^{234}Th residence times. This stratified scenario has

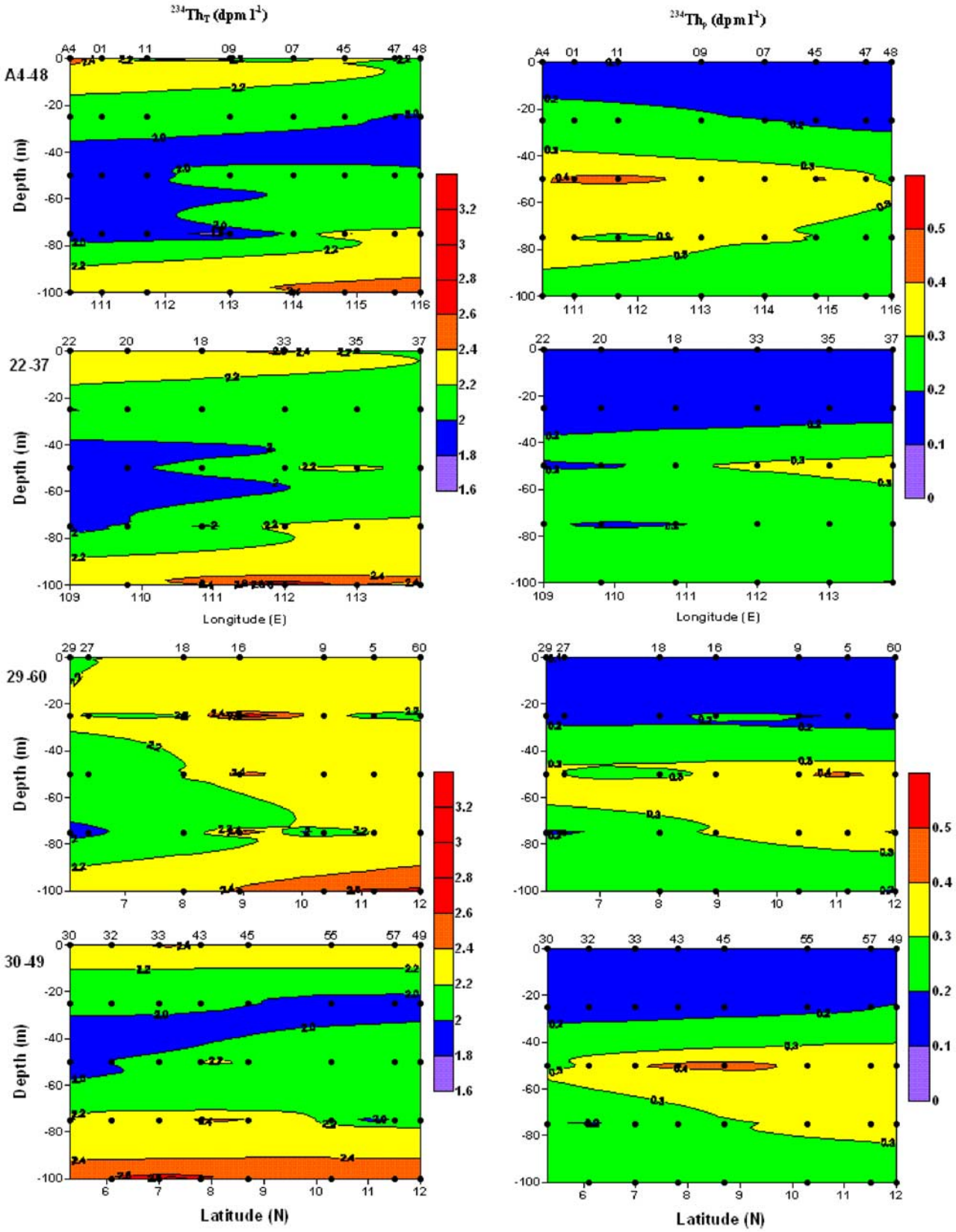

Figure 4. Depth-related variations in the total ^{234}Th (left panels) and particulate ^{234}Th (right panels) for 4 typical sections. The names of the sections and the station numbers are shown on the left and with the upper values separately. Sampling depths are indicated by filled dots. Values are in dpm l^{-1}.

been occasionally observed in other oceanographic settings, e.g., the North Pacific [*Coale and Bruland*, 1987].

[15] Overall, the subsurface minima in total ^{234}Th along the boundary of the study area were more prominent than in the central basin. This trend is concurrent with the general circulation pattern of the southern SCS in this season. Previous studies have shown that during the spring intermonsoon, the southern SCS is dominated by an anticyclonic gyre. This anticyclonic gyre is thought to be caused by the relaxation of the NE monsoon, which starts in the boreal winter and continues until spring in the following year [*Fang et al.*, 2002]. Coastal upwelling is then induced along the southwestern boundary of the SCS (see Figure 3), thus may increase the nutrient input from below the euphotic zone. As a consequence, enhanced export production and hence ^{234}Th scavenging rates in this regime are expected.

[16] In most cases, a subsurface maximum was evident in the depth profile of particulate ^{234}Th (Figure 4). This subsurface maximum is believed to be linked to the pigment maximum in the euphotic zone, a well documented and prominent feature of the oligotrophic SCS [e.g., *Ning et al.*, 2004]. However, it is important to note that the particulate ^{234}Th maximum was not necessarily coincident with the total ^{234}Th minimum.

3.3. Horizontal Distribution of ^{234}Th

[17] A prominent feature in the geographical distribution of surface ^{234}Th is associated with a low total ^{234}Th surface "tongue", which extends northwestward from the southeast corner of the study regime (Figure 5). Away from the "tongue", surface total ^{234}Th activities were slightly lower than, or within errors, equal to ^{238}U activities. Notably, the low ^{234}Th "tongue" was concurrent with the low temperature, low salinity plume that is thought to be associated with the intrusion of surface water from Sulu Sea through Balabac Strait (Figure 3). Below the surface, the distribution pattern of total ^{234}Th changed drastically with depth. At 25 m, enhanced depletion in ^{234}Th was observed in the east. Overall, this trend is consistent with the surface pattern of total ^{234}Th. In contrast, the distributions of total ^{234}Th at 50 and 75 m showed enhanced ^{234}Th scavenging in the west. At the 100 m horizon, total ^{234}Th activities were generally in equilibrium with ^{238}U.

[18] Another notable feature of the total ^{234}Th distribution below the surface was the substantial ^{234}Th excess relative to ^{238}U observed at some locations. For instance, at the 25 m horizon, total ^{234}Th activity at Station 16 was as high as 2.99 dpm l^{-1}. At the 75 m horizon, total ^{234}Th activity at Station 40 was even higher, up to 3.44 dpm l^{-1} (Figure 5). Similar phenomena have been observed below the euphotic zone elsewhere, and were interpreted as a result of particle remineralization [e.g., *Benitez-Nelson et al.*, 2001a; *Buesseler et al.*, 2005; *Savoye et al.*, 2004; *Usbeck et al.*, 2002]. Compared to these studies, the ^{234}Th excess observed in the southern SCS was significantly shallower. Interestingly, the ^{234}Th excess maximum at the 75 m horizon was right below the surface ^{234}Th depletion maximum. This indicates that most particles sinking from the surface were effectively remineralized within, rather than being exported out of the euphotic zone.

[19] As shown in Figure 5, surface particulate ^{234}Th activities were low and relatively uniform. Below the surface, enhanced particulate ^{234}Th activities were generally observed in the north of the study area. Notably, high particulate ^{234}Th activities were not necessarily coincident with low total ^{234}Th activities, indicating possible decoupling between elemental partitioning and POC export.

3.4. Particulate Organic Carbon

[20] POC concentrations ranged from a low of 0.4 μmol l^{-1} to a high of 8.7 μmol l^{-1}. The highest POC was roughly concurrent with the total ^{234}Th minimum in the surface (Table 1). Meanwhile, POC concentrations were lower than 3 μmol l^{-1} in most cases. At the surface, high POC concentrations were observed in the southeast, roughly coincident with the low temperature, low salinity plume (Figure 3). Another general feature is that the POC concentrations were higher in the surface waters and in the nearshore stations, and decreased with depth. It should also be noted that the regional patterns of POC were very different from those of particulate ^{234}Th, indicating that particulate ^{234}Th activity may not be solely controlled by the POC concentration (Table 1).

4. Discussion

4.1. Thorium-234 Export Fluxes

[21] In order to determine the flux of ^{234}Th from the upper ocean, and hence the extent of POC export, the following ^{234}Th activity balance equation is used:

$$\partial A_{Th}/\partial t = A_U\lambda - A_{Th}\lambda - P + V \quad (1)$$

where $\partial A_{Th}/\partial t$ is the change rate of total ^{234}Th activity, A_U is the ^{238}U activity, A_{Th} is the total ^{234}Th activity, λ is the decay constant (0.02876 d^{-1} for ^{234}Th), P is the net removal flux of ^{234}Th on particles, and V is the sum of advection and diffusion terms. In the open ocean, the magnitude of P is determined mostly by the extent of the ^{234}Th/^{238}U disequilibrium. Steady State (SS) is often assumed ($\partial A_{Th}/\partial t = 0$) and physical processes are ignored.

[22] The Nonsteady state (NSS) ^{234}Th formulation is believed necessary during plankton blooms, when significant ^{234}Th removal can occur [*Buesseler et al.*, 1998]. SS models are sufficient, however, when SS ^{234}Th fluxes are low, i.e., <800 dpm m^{-2} d^{-1} [*Savoye et al.*, 2006]. As will be demonstrated below, SS fluxes of ^{234}Th in this study were mostly $\leq$800 dpm m^{-2} d^{-1}. As such, we neglect the NSS term in the following flux calculations.

[23] The V term in equation (1) includes vertical and horizontal advection and diffusion processes. Vertical processes have been demonstrated to be significant in areas of intense upwelling, such as in the Equatorial Pacific and along the coast of the Arabian Sea during the SW monsoon [*Buesseler et al.*, 1995, 1998]. Horizontal ^{234}Th transport, meanwhile, can be important in coastal regions, especially in bays, where large horizontal gradients in ^{234}Th scavenging can occur [*Benitez-Nelson et al.*, 2000; *Charette et al.*, 2001]. The significance of physical processes in the calculation of ^{234}Th fluxes has been assessed in a recent review paper by *Savoye et al.* [2006].

[24] We have developed a regional three-dimensional (3-D) flux model that includes seasonal and site specific upwelling and horizontal fluxes in the overall regional

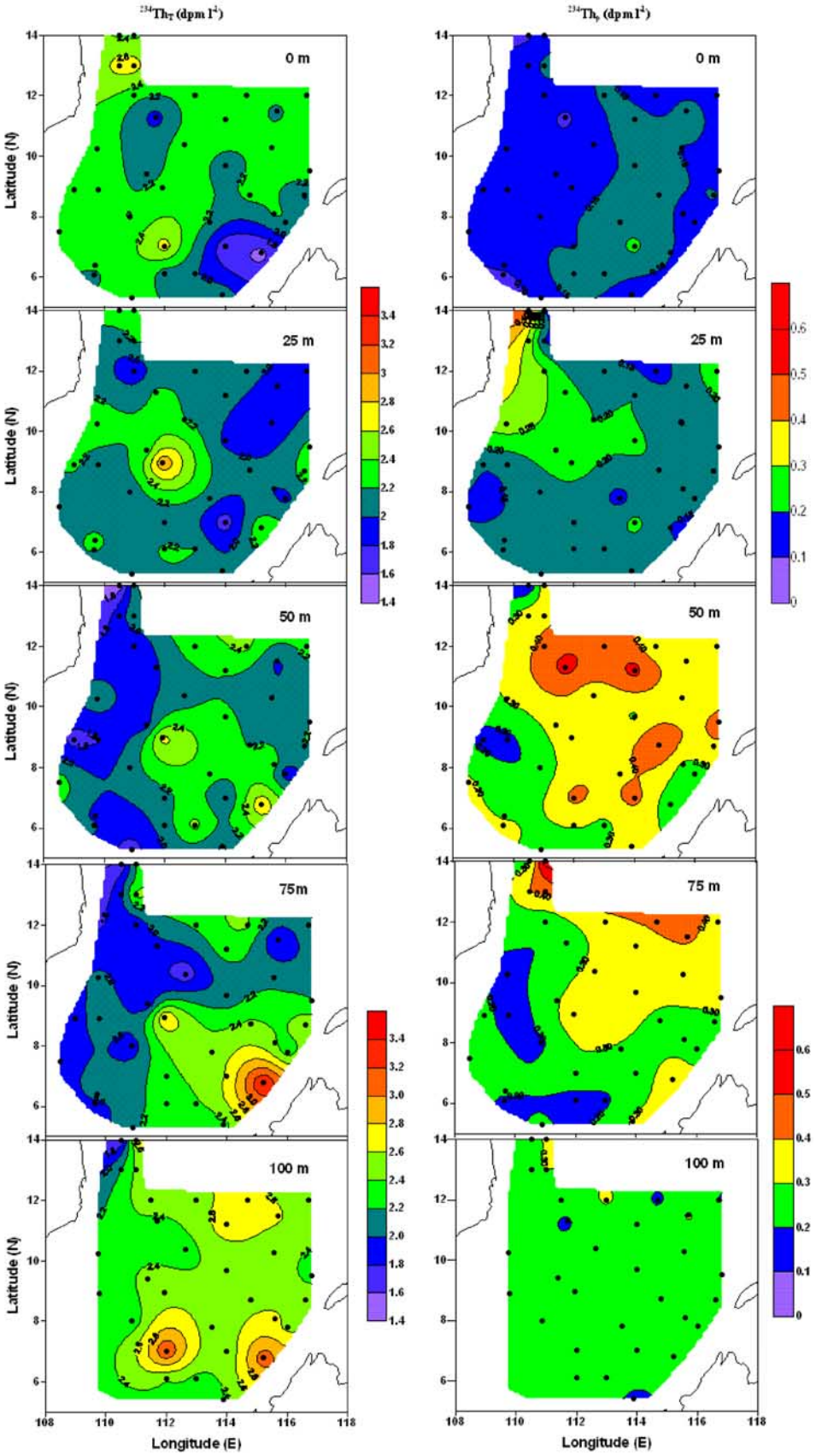

Figure 5. Contour plots of total ^{234}Th (left panels) and particulate ^{234}Th (right panels) at 0, 25, 50, 75, and 100 m depth horizons. Station locations are shown as filled dots. Values are in dpm l^{-1}.

Table 2. ^{234}Th Fluxes, POC/^{234}Th Ratios and POC Export Fluxes in the Upper Southern South China Sea

Station	Depth, m	SS Term[a] (dpm m^{-2} d^{-1})	HT Term[a] (dpm m^{-2} d^{-1})	VT Term[a] (dpm m^{-2} d^{-1})	Net ^{234}Th Flux (dpm m^{-2} d^{-1})	POC/^{234}Th, μmol dpm^{-1}	POC Flux, mmolC m^{-2}d^{-1}
A2	100	1668 ± 93	21.2	0.2	1689 ± 93	6.17 ± 0.24	10.4 ± 0.7
A4	100	939 ± 95	34.7	1.2	975 ± 95	5.99 ± 0.27	5.8 ± 0.6
01	100	1290 ± 100	15.2	0.7	1306 ± 100	6.62 ± 0.26	8.6 ± 0.7
09	100	948 ± 109	−6.7	0.9	942 ± 109	5.48 ± 0.44	5.2 ± 0.7
07	100	834 ± 102	−12.6	0.1	822 ± 102	4.86 ± 0.42	4.0 ± 0.6
11	100	1011 ± 88	22.3	0.3	1034 ± 88	6.68 ± 0.38	6.9 ± 0.7
13	100	563 ± 96	42.8	0.0	606 ± 96	6.92 ± 0.31	4.2 ± 0.7
15	100	982 ± 103	−8.0	−0.3	974 ± 103	1.45 ± 0.13	1.4 ± 0.2
16	100	−872 ± 126	−1.6	−0.1	−874 ± 126	3.17 ± 0.23	−2.8 ± 0.4
18	100	1020 ± 95	32.2	0.4	1053 ± 95	7.83 ± 0.55	8.2 ± 0.9
20	100	910 ± 99	−11.8	0.3	899 ± 99	7.12 ± 0.64	6.4 ± 0.9
22	75	838 ± 93	0.9	0.1	839 ± 93	9.43 ± 0.66	7.9 ± 1.0
25	75	537 ± 93	−40.7	0.6	497 ± 93	8.11 ± 0.65	4.0 ± 0.8
27	75	566 ± 96	2.8	0.3	569 ± 96	7.67 ± 0.49	4.4 ± 0.8
29	75	680 ± 85	7.7	0.2	688 ± 85	7.89 ± 0.39	5.4 ± 0.7
30	75	857 ± 87	−2.4	0.5	855 ± 87	9.19 ± 0.79	7.9 ± 1.0
32	100	595 ± 99	−43.0	0.0	552 ± 99	8.83 ± 0.58	4.9 ± 0.9
33	100	179 ± 98	−10.0	0.5	170 ± 98	5.76 ± 0.31	1.0 ± 0.6
35	100	323 ± 87	−21.7	0.2	302 ± 87	7.84 ± 0.39	2.4 ± 0.7
37	100	780 ± 93	28.4	−0.3	808 ± 93	8.74 ± 0.55	7.1 ± 0.9
40	100	−929 ± 130	−77.8	−0.7	−1008 ± 130	10.57 ± 0.60	−10.7 ± 1.5
42	100	991 ± 96	57.4	−0.4	1048 ± 96	4.81 ± 0.42	5.0 ± 0.6
43	100	343 ± 127	28.8	−0.1	372 ± 127	3.36 ± 0.24	1.2 ± 0.4
45	100	419 ± 123	25.9	0.2	445 ± 123	3.77 ± 0.29	1.7 ± 0.5
47	100	395 ± 117	−21.5	0.1	374 ± 117	5.36 ± 0.26	2.0 ± 0.6
48	100	849 ± 116	−138.0	−0.4	711 ± 116	3.45 ± 0.28	2.5 ± 0.4
51	100	258 ± 103	−70.1	−0.1	188 ± 103	4.44 ± 0.14	0.8 ± 0.5
53	100	453 ± 111	14.8	0.5	468 ± 111	5.27 ± 0.31	2.5 ± 0.6
55	100	974 ± 106	−15.1	0.6	960 ± 106	5.08 ± 0.15	4.9 ± 0.6
57	100	1163 ± 102	−23.2	1.6	1141 ± 102	11.00 ± 0.14	12.6 ± 1.1
49	100	585 ± 123	−18.0	0.9	568 ± 123	8.69 ± 0.74	4.9 ± 1.1
60	100	62 ± 100	−18.9	0.8	44 ± 100	6.72 ± 0.59	0.3 ± 0.7
05	100	308 ± 108	−26.3	1.0	283 ± 108	7.93 ± 0.17	2.2 ± 0.9
03	100	198 ± 126	14.6	0.4	213 ± 126	3.75 ± 0.02	0.8 ± 0.5
B2	100	172 ± 108	25.8	1.1	199 ± 108	4.88 ± 0.34	1.0 ± 0.5
B4	100	284 ± 100	5.3	0.2	290 ± 100	5.92 ± 0.15	1.7 ± 0.6

[a]SS, HT, and VT terms are defined as the ^{234}Th fluxes driven by ^{234}Th/^{238}U disequilibria, horizontal transport, and vertical transport processes, respectively; see the text for details.

^{234}Th activity balance. In this case, the particle flux P_{Th} can be solved from the following equation with the steady state assumption:

$$P_{Th} = A_U\lambda_{Th} - A_{Th}\lambda_{Th} - u\cdot\partial A_{Th}/\partial x - v\cdot\partial A_{Th}/\partial y - w\cdot\partial A_{Th}/\partial z + K_x\cdot\partial^2 A_{Th}/\partial x^2 + K_y\cdot\partial^2 A_{Th}/\partial y^2 + K_z\cdot\partial^2 A_{Th}/\partial z^2 \quad (2)$$

where u is the zonal velocity and $\partial A_{Th}/\partial x$ the activity gradient from west to east, v is the meridional velocity and $\partial A_{Th}/\partial y$ the activity gradient from south to north, and w is the upwelling velocity and $\partial A_{Th}/\partial z$ the vertical gradient in ^{234}Th activity; K_x, K_y, and K_z are the zonal, meridional, and vertical diffusivities, respectively, and $\partial^2 A_{Th}/\partial x^2$, $\partial^2 A_{Th}/\partial y^2$, and $\partial^2 A_{Th}/\partial z^2$, the second derivative of the activity distribution. To fully understand the relative importance of ^{234}Th/^{238}U disequilibria and physical processes in derived ^{234}Th export, we follow *Benitez-Nelson et al.* [2000] and break equation (2) into several mathematical terms, where $(A_U\text{-}A_{Th})\lambda_{Th}$ is defined as the SS term, $-u\cdot\partial A_{Th}/\partial x - v\cdot\partial A_{Th}/\partial y + K_x\cdot\partial^2 A_{Th}/\partial x^2 + K_y\cdot\partial^2 A_{Th}/\partial y^2$ is defined as the horizontal transport (HT) term, and $-w\cdot\partial A_{Th}/\partial z + K_z\cdot\partial^2 A_{Th}/\partial z^2$, the vertical transport (VT) term.

[25] The physical transport parameters were derived from a 3-D nonlinear Princeton Ocean Model developed by *Blumberg and Mellor* [1987]. Our model domain covers the area between 103°E to 139°E and 8°S to 47°N, with a horizontal grid resolution of 0.25° × 0.25° and 21 σ-levels in the vertical dimension. The model was driven with the climatological wind stress and net heat flux through sea-air interface using data from World Ocean Atlas 2001 [*Conkright et al.*, 2002] and the outputs of a global ocean model [*Yu et al.*, 2002] on an open boundary. Our ^{234}Th data were placed onto the model grid by using a linear kriging technique, the same as that employed in Figures 3 to 5. The upwelling velocity at the surface was set to be zero. The ^{234}Th transport caused by physical processes was evaluated through integrating the model for 1 day with a time step of 20 min. Finally, P_{Th} was determined in all four layers (0–25, 25–50, 50–75, and 75–100 m), and the net flux at the bottom of the euphotic zone was calculated as the sum of the fluxes from above layers. In cases where the bottom depth is less than 150 m, ^{234}Th fluxes at the 75 m horizon were calculated.

[26] Model results are presented in Table 2. In general, the magnitude of the vertical ^{234}Th flux was dominated by the SS term, i.e., particle scavenging. The VT term ranged from −0.7 to 1.6 dpm m^{-2} d^{-1}. This is obviously a negligible term since it is within the uncertainty of the net ^{234}Th export flux. *Buesseler et al.* [1995], meanwhile, found

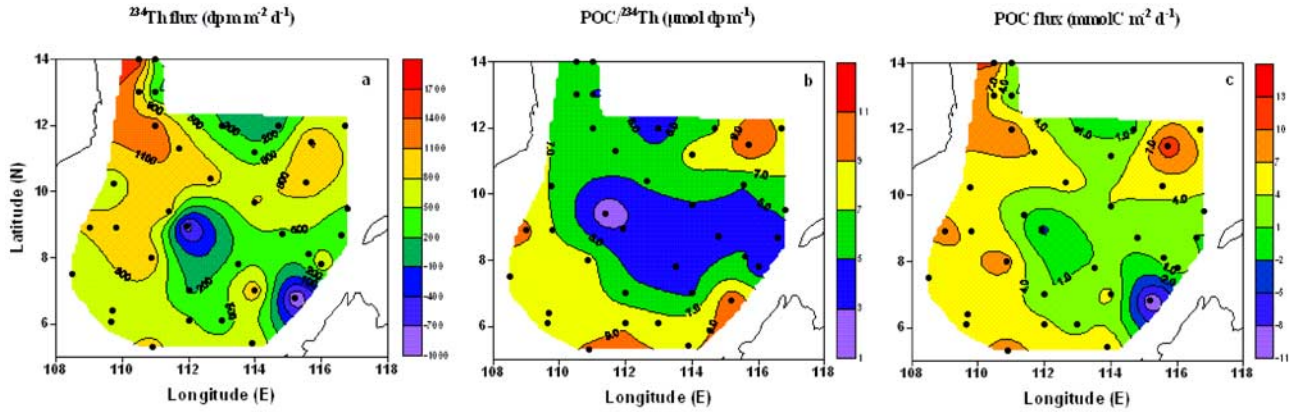

Figure 6. Contour plots of (a) particulate ^{234}Th flux (dpm m^{-2} d^{-1}), (b) POC/^{234}Th ratio (μmol dpm^{-1}), and (c) POC export flux (mmolC m^{-2} d^{-1}) at the export horizon. Station locations are shown as filled dots.

that over the equatorial upwelling region, the incorporation of the VT term in the ^{234}Th model increased ^{234}Th flux by as much as 50%. The contrasting role of the VT term between this study and *Buesseler et al.* [1995] is presumably due to the fact that in the spring, the upwelling velocity w, as well as the vertical activity gradient $\partial A_{Th}/\partial z$, is dramatically lower in the southern SCS than in the equatorial upwelling region.

[27] The HT term varied between −138 and 57.4 dpm m^{-2} d^{-1}. In general, it accounted for less than 10% of the overall ^{234}Th balance, and was usually below the overall uncertainty of the net ^{234}Th export flux. In cases where the SS ^{234}Th fluxes were low, however, the contribution of the ^{234}Th flux from horizontal transport is much more significant. For instance, at Station 60, where the SS term was as low as 62 ± 100 dpm m^{-2} d^{-1}, the incorporation of the horizontal processes reduced the net ^{234}Th export fluxes by as much as 30%. At Station B2, the addition of the HT term resulted in a 15% increase in the SS ^{234}Th export flux of 172 ± 108 dpm m^{-2} d^{-1}. In comparison, *Charette et al.* [2001] investigated the ^{234}Th export fluxes in the Gulf of Maine and found that the inclusion of horizontal advection and diffusion fluxes to the 1-D model acted to increase the ^{234}Th fluxes by an average of ∼10%. *Gustafsson et al.* [1998] reported that incorporation of horizontal transport of ^{234}Th increased particulate ^{234}Th fluxes by a factor of 3 in Casco Bay, Maine.

[28] The ^{234}Th fluxes derived from the 3-D model followed a pattern similar to the ^{234}Th deficit (Figure 6a). In general, fluxes were ≤1000 dpm m^{-2} d^{-1}, indicating relatively modest particle scavenging in the oligotrophic southern SCS. Along the western and southern boundaries of the study region, ^{234}Th fluxes were relatively higher. The highest flux was found in the northernmost station, A2 (∼1700 dpm m^{-2} d^{-1}). Next to A2, the ^{234}Th flux dropped to <300 dpm m^{-2} d^{-1} at B4. Around 7°N 115°E there occurred a tongue of low ^{234}Th fluxes (<500 dpm m^{-2} d^{-1}), extending northwestward to ∼9°N 111°E. For instance, at Station 16 and 40, ^{234}Th fluxes were determined to be −874 ± 126 and −1008 ± 130 dpm m^{-2} d^{-1}, respectively.

[29] A few investigators have observed ^{234}Th excess relative to ^{238}U below the mixed layer, which was interpreted as the result of particle break-up and remineralization [*Benitez-Nelson et al.*, 2001a; *Savoye et al.*, 2004]. Since ^{234}Th is supposed to be added to the seawater solely through the in situ decay of ^{238}U, in a closed system, the integrated ^{234}Th excess below the mixed layer should be equal to or lower than the integrated ^{234}Th deficit in the mixed layer. This implies that mesopelagic ^{234}Th flux should be zero or positive. Negative flux at depth thus indicates either an extra ^{234}Th source from elsewhere in the study region, or that the steady state assumption is not valid. Meanwhile, a comparison of the residence times of ^{234}Th and ^{228}Th revealed that the vertical distributions of both nuclides are under steady state in this season [*Cai et al.*, 2006c]. Therefore a possible process that caused a negative ^{234}Th flux is the lateral input of particulate matter. Lateral transport of particulate matter could potentially remove ^{234}Th from one region to another, thus resulting in ^{234}Th deficits or excess along a horizontal axis.

[30] One of the consequences of the lateral transport of particulate matter and the associated ^{234}Th is that the model-derived ^{234}Th fluxes (and hence POC export rates) may be either overestimated or underestimated. This is because when using ^{234}Th to quantify POC export flux, we essentially assume that ^{234}Th removal in the euphotic zone is solely driven by the vertical settling of sinking particles. This assumption, as shown here, is certainly questionable. Meanwhile, through high-resolution sampling, the bias in model-derived ^{234}Th export fluxes as demonstrated in this study can be minimized by integrating the ^{234}Th deficit and excess over the whole study region.

4.2. Particulate Organic Carbon/^{234}Th Ratios

[31] The export flux of POC can be calculated as the product of the model-derived ^{234}Th flux and the POC/^{234}Th ratio measured on sinking particles. This approach assumes that POC and particulate ^{234}Th have the same mean sinking velocity at the export horizon [*Smith et al.*, 2006]. Previous studies have shown that POC/^{234}Th ratios may vary by as much as three orders of magnitude depending on region, depth, and season [*Buesseler et al.*, 2006]. Moreover, this ratio has been found to vary depending upon whether filters of small or large pore diameters were employed, or if

sediment traps were used for the determination of POC/^{234}Th ratios (for summary see *Buesseler et al.* [2006]). Most recently, *Cai et al.* [2006c] demonstrated that the variation in POC/^{234}Th ratios with particle size can be interpreted as the result of a combination of ^{234}Th decay and the remineralization of POC during particle aggregation.

[32] In this study, POC/^{234}Th ratio was only determined on suspended particles due that we did not have ship time for deployment of an in situ pump to sample size-fractionated particles. At the export horizon, POC/^{234}Th ratio on suspended particles ranged from 1.45 ± 0.13 μmol dpm^{-1} to 11.0 ± 0.14 μmol dpm^{-1} (Table 2) with an average of 6.4 ± 2.2 μmol dpm^{-1}. This POC/^{234}Th ratio is generally comparable to the results in the Southern Ocean and the North Atlantic (5∼10 μmol dpm^{-1}) [*Buesseler et al.*, 1992, 2001] but lower than in the Gulf of Maine (∼15 μmol dpm^{-1}) [*Benitez-Nelson et al.*, 2000; *Gustafsson et al.*, 1998].

[33] From Figure 6b, we can see that POC/^{234}Th ratios follow a pattern similar to ^{234}Th fluxes, with a tongue of low POC/^{234}Th ratio (<5.0 μmol dpm^{-1}) extending northwestward from ∼9°N 116°E to ∼10°N 111°E. Along the western and southern boundaries, POC/^{234}Th ratios were higher (>7.0 μmol dpm^{-1}). The similarity in the geographic distributions of ^{234}Th flux and POC/^{234}Th ratio is rather unexpected yet interesting given that these two parameters are thought to be controlled by different processes.

[34] Many studies have shown significant differences in the POC/^{234}Th as a result of sampling technique (for a review, see *Buesseler et al.* [2006]). *Moran et al.* [1999] suggested that bottle derived POC data may overestimate true POC levels, due in part to adsorption of dissolved organic carbon (DOC) onto the filter and hence a high filter blank. These researchers found POC concentrations to be 2–4 times higher in small volume (∼1–2 L) versus large volume (∼100–600 L) samples. In a recent study, *Liu et al.* [2005] vigorously compared in situ pump and bottle POC at different sites, and found elevated bottle POC concentrations. With a correction of DOC blank, they concluded that the preferential capture of living zooplankton by marine sampling bottles is the major cause for higher bottle POC. In the present study, the effect of DOC adsorption on the bottle POC/^{234}Th ratio may be minimized due to the fact that a volume of up to 6–8 L of seawater was filtered onto a 25 mm QMA filter with an effective dimension of ∼20 mm. This is equivalent to a volume of ∼300–400 L of seawater pumped through a 142 mm QMA filter.

[35] A number of researchers have used POC/^{234}Th ratio on large particles (>53 μm or >70 μm) to convert ^{234}Th fluxes into POC export rates [e.g., *Buesseler et al.*, 1998; *Cochran et al.*, 2000]. Unfortunately, size-fractionated POC/^{234}Th ratios were not determined in this cruise. Depth profiles of size-fractionated POC/^{234}Th ratio collected from the northern SCS, meanwhile, showed that POC/^{234}Th ratio at 100 m decrease slightly with particle size. In addition, bottle POC/^{234}Th ratios were consistently higher than those determined on pump samples [Chen et al., in preparation]. Using higher POC/^{234}Th ratios based on our bottle samples will, therefore, allow us to place a constraint on the upper limit of the export fluxes of POC in the study area.

4.3. Particulate Organic Carbon Export Fluxes

[36] POC export fluxes in the southern SCS varied from a low of −10.7 ± 1.5 mmolC m^{-2} d^{-1} to a high of 12.6 ± 1.1 mmolC m^{-2} d^{-1} (Table 2), with an average of 3.8 ± 4.0 mmolC m^{-2} d^{-1} (±1SD, n = 36). Errors were determined from the propagation of uncertainties associated with the model-derived ^{234}Th flux and the measured POC/^{234}Th ratio. A negative flux implies net POC input via lateral transport of particulate matter from nearby waters. As expected, the overall pattern in POC export flux is similar to the patterns in ^{234}Th flux. High POC export fluxes tended to occur along the western and the southern boundaries. A tongue of low POC flux was found to extend northwestward from ∼7°N 116°E to ∼10°N 111°E (Figure 6c).

[37] There are few historical measurements of POC export fluxes or new production in the southern SCS. *Chen et al.* [1998] attempted to use data from 9 sets of deep sediment traps (>1000 m) deployed in the central SCS to estimate the POC export flux from the upper 100 m. Using the "Martin Curve", average export production was back-calculated, ranging from 1.0 to 3.3 mmolC m^{-2} d^{-1} during the deployment period from December 1990 to April 1995. *Cai et al.* [2002a] evaluated the POC export flux at a single station (06°00.94′N, 110°01.26′E) in the southern SCS. By applying a multitracer (^{234}Th and ^{228}Th) approach, the POC export rate was constrained to be ∼ 1.7–5.7 mmolC m^{-2} d^{-1}. In another study, *Cai et al.* [2002b] collected three depth profiles of ^{228}Ra and NO_3^- from the upper 300 m of the water column in this region. By using a 1-D diffusion-decay model, these investigators were able to assess the nutrient budget in the euphotic zone. New production rates were determined to be 4.4, 5.1, and 5.7 mmolC m^{-2} d^{-1} at these sites. *Chen* [2005] investigated the spatial and temporal variations in new production and primary production in the northern SCS. On the basis of the ^{15}N incubation technique, new production rates over the basin were determined to be ∼5.8 mmolC m^{-2} d^{-1} in the spring. All these values are overall in agreement with our estimate of POC export rate that is 3.8 ± 4.0 mmolC m^{-2} d^{-1} on average. It is interesting to note that in general, the new production rates are slightly higher than the POC export fluxes derived from sediment trap or from the ^{234}Th method. The reason causing this difference is unclear. The accumulation of dissolved organic carbon in the upper water column, as observed in the subtropical Pacific Ocean [*Benitez-Nelson et al.*, 2007], could be one of the plausible interpretations.

[38] The ratio of ^{234}Th-derived POC export to primary production was defined as the ThE ratio [*Buesseler*, 1998]. While primary production was not determined in this study, it is still useful to compare our ^{234}Th-derived POC export to reported primary production rates in order to place our results in context of other ^{234}Th-derived POC export studies. From SeaWiFS data, *Liu et al.* [2002] estimated a primary production rate of ∼25 mmolC m^{-2} d^{-1} over the upper 135 m in mid-May. This value is about 20% higher than their model-derived primary production rate of ∼21 mmolC m^{-2} d^{-1}. *Chen* [2005] derived an average primary production rate of 21.6 mmolC m^{-2} d^{-1} over the northern SCS basin for spring surveys that were conducted between 2000 and 2003. On the basis of these results, a first

order estimate for the ThE ratio would be ~17% for the southern SCS during the spring intermonsoon.

5. Summary

[39] With the aid of a modified small-volume MnO_2 co-precipitation technique, we were able to derive, for the first time, high-resolution, high-precision spatial distributions of ^{234}Th and hence POC export in one of the largest marginal seas in the world, the South China Sea. The stratified structure of ^{234}Th/^{238}U disequilibria indicates that the euphotic zone in this region can be separated into an upper layer and a lower layer.

[40] To better understand the role of physics in ^{234}Th distributions, a three-dimensional steady state model was used to assess the relative importance of physical processes in the overall ^{234}Th balance. It was found that horizontal and vertical processes generally accounted for a small term in the flux calculation of ^{234}Th. Using the 3-D model of ^{234}Th fluxes and the measurements of POC/^{234}Th ratio on suspended particles, we were allowed to place a constraint on the upper limit of the export fluxes of POC. During the spring intermonsoon, POC export at 100 m in the southern SCS was on the order of -10.7 ± 1.5–12.6 ± 1.1 mmolC m^{-2} d^{-1}, with an average of 3.8 ± 4.0 mmolC m^{-2} d^{-1}. Negative fluxes could be caused by the lateral input of particulate matter from nearby waters. The regional pattern in the POC export is concurrent with the overall circulation pattern in this season.

[41] The ^{234}Th-derived POC export in this study was found to be in general agreement with the historical measurements of moored sediment-trap POC fluxes and of nitrate-based new production. This provides confidence that the ^{234}Th approach is a relatively simple and robust method for determining POC export fluxes from the upper ocean. The uncertainty associated with the estimated POC export depends mostly on how accurately we can characterize POC/^{234}Th ratio on sinking particles. In this study, POC/^{234}Th ratios on suspended particles were used to convert the ^{234}Th fluxes into POC export rates. To derive more accurate estimates of POC export, future studies aimed at better constraining the "flux-weighted POC/^{234}Th ratio" [*Buesseler et al.*, 2006] are warranted.

[42] **Acknowledgments.** We wish to thank the crew of R/V "Shiyan 3" for their assistance in sample collection during the cruise. This work was supported by the Natural Science Foundation of China (NSFC) through grants 90211020, 40206011, 40676066, 40490260, 40521003 and 40676045, and by the Ministry of Education through the Program for Changjiang Scholars and Innovative Research Team in University.

References

Bacon, M. P., J. K. Cochran, D. Hirschberg, T. R. Hammar, and A. P. Fleer (1996), Export flux of carbon at the equator during the EqPac time-series cruises estimated from Th-234 measurements, *Deep Sea Res., Part II*, *43*, 1133–1153.

Benitez-Nelson, C. R., K. O. Buesseler, and G. Crossin (2000), Upper ocean carbon export, horizontal transport, and vertical eddy diffusivity in the southwestern Gulf of Maine, *Cont. Shelf Res.*, *20*, 707–736.

Benitez-Nelson, C., K. O. Buesseler, D. M. Karl, and J. Andrews (2001a), A time-series study of particulate matter export in the North Pacific Subtropical Gyre based on Th-234: U-238 disequilibrium, *Deep Sea Res., Part I*, *48*, 2595–2611.

Benitez-Nelson, C. R., K. O. Buesseler, M. M. Rutgers van der Loeff, J. A. Andrews, L. Ball, G. Crossin, and M. A. Charette (2001b), Testing a new small-volume technique for determining thorium-234 in seawater, *J. Radioanal. Nucl. Chem.*, *248*, 795–799.

Benitez-Nelson, C. R., et al. (2007), Mesoscale eddies drive increased silica export in the subtropical Pacific Ocean, *Science*, *312*, 1017–1021.

Blumberg, A. F., and G. L. Mellor (1987), A description of a three-dimensional coastal ocean circulation model, in *Three-Dimensional Coastal Ocean Models*, edited by N. S. Heaps, p. 208, AGU, Washington, D. C.

Buesseler, K. O. (1998), The decoupling of production and particulate export in the surface ocean, *Global Biogeochem. Cycles*, *12*, 297–310.

Buesseler, K., M. P. Bacon, J. K. Cochran, and H. D. Livingston (1992), Carbon and nitrogen export during the JGOFS North Atlantic bloom experiment estimated from ^{234}Th:^{238}U disequilibria, *Deep Sea Res., Part I*, *39*, 1115–1137.

Buesseler, K. O., J. A. Andrews, M. C. Hartman, R. Belastock, and F. Chai (1995), Regional estimates of the export flux of particulate organic carbon derived from thorium-234 during the JGOFS EqPac program, *Deep Sea Res., Part II*, *42*, 777–804.

Buesseler, K., L. Ball, J. Andrews, C. Benitez-Nelson, R. Belastock, F. Chai, and Y. Chao (1998), Upper ocean export of particulate organic carbon in the Arabian Sea derived from thorium-234, *Deep Sea Res., Part II*, *45*, 2461–2487.

Buesseler, K. O., C. Benitez-Nelson, M. Rutgers van der Loeff, J. Andrews, L. Ball, G. Crossin, and M. Charette (2001), An intercomparison of small- and large-volume techniques for thorium-234 in seawater, *Mar. Chem.*, *74*, 15–28.

Buesseler, K. O., J. E. Andrews, S. M. Pike, M. A. Charette, L. E. Goldson, M. A. Brzezinski, and V. P. Lance (2005), Particle export during the Southern Ocean Iron Experiment (SOFeX), *Limnol. Oceanogr.*, *50*, 311–327.

Buesseler, K. O., et al. (2006), An assessment of particulate organic carbon to thorium-234 ratios in the ocean and their impact on the application of ^{234}Th as a POC flux proxy, *Mar. Chem.*, *100*, 213–233.

Cai, P., Y. Huang, M. Chen, L. Guo, G. Liu, and Y. Qiu (2002a), New production based on ^{228}Ra-derived nutrient budgets and thorium-estimated POC export at the intercalibration station in the South China Sea, *Deep Sea Res., Part I*, *49*, 53–66.

Cai, P., Y. Huang, M. Chen, G. Liu, Y. Qiu, and M. Cai (2002b), New production in the South China Sea: A coupled ^{228}Ra-nitrate approach, *Sci. China Ser. D*, *45*, 103–109.

Cai, P., M. Dai, D. Lv, and W. Chen (2006a), An improvement in the small-volume technique for determining thorium-234 in seawater, *Mar. Chem.*, *100*, 282–288.

Cai, P., M. Dai, D. Lv, and W. Chen (2006b), How accurate are ^{234}Th measurements in seawater based on the MnO_2-impregnated cartridge technique?, *Geochem. Geophys. Geosyst.*, *7*, Q03020, doi:10.1029/2005GC001104.

Cai, P., M. Dai, W. Chen, T. Tang, and K. Zhou (2006c), On the importance of the decay of ^{234}Th in determining size-fractionated C/^{234}Th ratio on marine particles, *Geophys. Res. Lett.*, *33*, L23602, doi:10.1029/2006GL027792.

Charette, M. A., S. B. Moran, and J. K. B. Bishop (1999), Th-234 as a tracer of particulate organic carbon export in the subarctic northeast Pacific Ocean, *Deep Sea Res., Part II*, *46*, 2833–2861.

Charette, M. A., S. B. Moran, S. M. Pike, and J. N. Smith (2001), Investigating the carbon cycle in the Gulf of Maine using the natural tracer thorium-234, *J. Geophys. Res.*, *106*, 11,553–11,579.

Chen, Y. L. (2005), Spatial and seasonal variations of nitrate-based new production and primary production in the South China Sea, *Deep Sea Res., Part I*, *52*, 319–340.

Chen, J. H., R. L. Edwards, and G. J. Wasserburg (1986), ^{238}U, ^{234}U and ^{232}Th in seawater, *Earth Planet. Sci. Lett.*, *80*, 241–251.

Chen, J., L. Zheng, M. Wiesner, R. Chen, Y. Zheng, and H. Wong (1998), Estimations of primary production and export production in the South China Sea based on sediment trap experiments, *Chinese Sci. Bull.*, *43*, 583–586.

Coale, K. H., and K. W. Bruland (1985), ^{234}Th/^{238}U disequilibria within the California current, *Limnol. Oceanogr.*, *30*, 22–33.

Coale, K. H., and K. W. Bruland (1987), Oceanic stratied euphotic zone as elucidated by ^{234}Th:^{238}U disequilibria, *Limnol. Oceanogr.*, *32*, 189–200.

Cochran, J. K., and P. Masque (2003), Short-lived U/Th series radionuclides in the ocean: Tracers for scavenging rates, export fluxes and particle dynamics, *Uranium-Series Geochem. Rev. Mineral. Geochem.*, *52*, 461–492.

Cochran, J. K., K. O. Buesseler, M. P. Bacon, H. W. Wang, D. J. Hirschberg, L. Ball, J. Andrews, G. Crossin, and A. Fleer (2000), Short-lived thorium isotopes (^{234}Th, ^{228}Th) as indicators of POC export and particle cycling in the Ross Sea, southern ocean, *Deep Sea Res., Part II*, *47*, 3451–3490.

Conkright, M. E., R. A. Locarnini, H. E. Garcia, T. D. O'Brien, T. P. Boyer, C. Stephens, and J. I. Antonov (2002), World ocean Atlas 2001: Objective analyses, data statistics, and figures CD-ROM documentation, in *National Oceanographic Data Center Internal Report 17*, p. 17, National Oceanographic Data Center, Silver Spring, MD.

Eppley, R. W., and B. J. Peterson (1979), Particulate organic matter flux and planktonic new production in the deep ocean, *Nature*, *282*, 677–680.

Fang, W., G. Fang, P. Shi, Q. Huang, and Q. Xie (2002), Seasonal structures of upper layer circulation in the southern South China from in situ observations, *J. Geophys. Res.*, *Oceans*, *107*(C11), 3202, doi:10.1029/2002JC001343.

Frankignoulle, M., and A. V. Borges (2001), European continental shelf as a significant sink for atmospheric carbon dioxide, *Global Biogeochem. Cycles*, *15*, 569–576.

Gustafsson, O., K. O. Buesseler, W. R. Geyer, S. B. Moran, and P. M. Gschwend (1998), An assessment of the relative importance of horizontal and vertical transport of particle-reactive chemicals in the coastal ocean, *Cont. Shelf Res.*, *18*, 805–829.

Hu, J., K. Hiroshi, H. Hong, and Y. Qu (2000), A review on the currents in the South China Sea: Seasonal circulation, South China Sea warm current and Kuroshio intrusion, *J. Oceanogr.*, *56*, 607–624.

Huang, Q. (1994), Distributions and variations of the temperature and salinity in the southern South China Sea, in *Proceedings of Physical Oceanography studies in the Nansha Islands Sea Area*, China Ocean Press, Beijing.

Kara, A. B., P. A. Rochford, and H. E. Hurlburt (2000), An optimal definition for ocean mixed layer depth, *J. Geophys. Res.*, *Oceans*, *105*, 16,783–16,801.

Knap, A., A. Michaels, A. Close, H. Ducklow, and A. Dickson (1996), Protocols for the Joint Global Ocean Flux Study (JGOFS) core measurements, JGOFS Report Nr. 19, vi-170 pp. (Reprint of the IOC Manuals and Guides No. 29, UNESCO 1994)

Liu, K. K., L. Atkinson, C. T. A. Chen, S. Gao, J. Hall, R. W. Macdonald, L. Talaue McManus, and R. Quiñones (2000), Exploring continental margin carbon fluxes on a global scale, *EOS Trans. Am. Geophys. Union*, *81*, 641–644.

Liu, Z., J. Xu, L. Li, and M. Shi (2001), Characteristics and distribution of water masses in the South China Sea during summer and winter of 1998, in *Oceanography in China* (in Chinese), edited by H. Xue, F. Chai, and J. Xu, pp. 221–230, China Ocean Press, Beijing.

Liu, K. K., S. Y. Chao, P. T. Shaw, G. C. Gong, C. C. Chen, and T. Y. Tang (2002), Monsoon-forced chlorophyll distribution and primary production in the South China Sea: Observations and a numerical study, *Deep Sea Res., Part I*, *49*, 1387–1412.

Liu, Z. F., G. Stewart, J. K. Cochran, C. Lee, R. A. Armstrong, D. J. Hirschberg, B. Gasser, and J. C. Miquel (2005), Why do POC concentrations measured using Niskin bottle collections sometimes differ from those using in-situ pumps?, *Deep Sea Res., Part I*, *52*, 1324–1344.

Moran, S. B., M. A. Charette, S. M. Pike, and C. A. Wicklaund (1999), Differences in seawater particulate organic carbon concentration in samples collected using small- and large- volume methods: The importance of DOC adsorption to the filter blank, *Mar. Chem.*, *67*, 33–42.

Murray, J. W., J. Young, J. Newton, J. Dunne, T. Chapin, and B. Paul (1996), Export flux of particulate organic carbon from the central Equatorial Pacific determined using a combined drifting trap-^{234}Th approach, *Deep Sea Res. Part II*, *43*, 1095–1132.

Ning, X., F. Chai, H. Xue, Y. Cai, C. Liu, and J. Shi (2004), Physical-biological oceanographic coupling influencing phytoplankton and primary production in the South China Sea, *J. Geophys. Res.*, *Oceans*, *109*, C10005, doi. 10.1029/2004JC002365.

Pike, S. M., K. O. Buesseler, J. A. Andrews, and N. Savoye (2005), Quantification of ^{234}Th recovery in small volume sea water samples by inductively coupled plasma mass spectrometry, *J. Radioanal. Nucl. Chem.*, *263*, 355–360.

Rutgers van der Loeff, M. M., K. Buesseler, U. Bathmann, I. Hense, and J. Andrews (2002), Comparison of carbon and opal export rates between summer and spring bloom periods in the region of the Antarctic Polar Front, SE Atlantic, *Deep Sea Res., Part II*, *49*, 3849–3869.

Savoye, N., K. O. Buesseler, D. Cardinal, and F. Dehairs (2004), ^{234}Th deficit and excess in the southern ocean during spring 2001: Particle export and remineralization, *Geophys. Res. Lett.*, *31*, L12301, doi:10.1029/2004GL019744.

Savoye, N., C. Benitez-Nelson, A. B. Burd, J. K. Cochran, M. Charette, K. O. Buesseler, G. A. Jackson, M. Roy-Barman, S. Schmidt, and M. Elskens (2006), ^{234}Th sorption and export models in the water column: A review, *Mar. Chem.*, *100*, 234–249.

Smith, J. N., S. B. Moran, and E. A. Speicher (2006), On the accuracy of upper ocean particulate organic carbon export fluxes estimated from ^{234}Th/^{238}U disequilibrium, *Deep Sea Res., Part I*, *53*, 860–868.

Tsunogai, S., S. Watanabe, and T. Sato (1999), Is there a "continental shelf pump" for the absorption of atmospheric CO_2?, *Tellus, Ser. B*, *51*, 701–712.

Usbeck, R., M. R. van der Loeff, M. Hoppema, and R. Schlitzer (2002), Shallow remineralization in the Weddell Gyre, *Geochem. Geophys. Geosyst.*, *3*(1), 1008, doi:10.1029/2001GC000182.

Waples, J. T., C. R. Benitez-Nelson, N. Savoye, M. Rutgers van der Loeff, M. Baskaran, and O. Gustafsson (2006), An Introduction to the application and future use of ^{234}Th in aquatic systems, *Mar. Chem.*, *100*, 166–189.

Yu, Y. Q., R. C. Yu, X. H. Zhang, and H. L. Liu (2002), A flexible global coupled climate model, *Adv. Atmos. Sci.*, *19*, 169–190.

P. Cai, W. Chen, M. Dai, Q. Li, D. Lv, T. Tang, and Z. Wan, State Key Laboratory of Marine Environmental Science, Xiamen University, 422 Siming Nanlu, Xiamen 361005, China. (mdai@xmu.edu.cn)

D. Wang, Key Laboratory of Tropical Marine Environmental Dynamics, South China Sea Institute of Oceanology, Chinese Academy of Sciences, Guangzhou, China.